High-Strength Biodegradable Poly(vinyl alcohol)/Fly Ash Composite Films

Dilip Chandra Deb Nath,[1] Sri Bandyopadhyay,[1] Philip Boughton,[1] Aibing Yu,[1] Darryl Blackburn,[2] Chris White[2]

[1]*School of Material Science and Engineering, University of New South Wales, Kensington, New South Wales, Australia*
[2]*Research and Ash Development, Cement Australia, Brisbane, Queensland, Australia*

Received 20 August 2009; accepted 11 October 2009
DOI 10.1002/app.31635
Published online 2 March 2010 in Wiley InterScience (www.interscience.wiley.com).

ABSTRACT: We prepared biodegradable composite films of poly(vinyl alcohol) (PVA) and fly ash (FA) spanning 5, 10, 15, 20, and 25 wt % concentrations by casting aqueous solutions. The tensile strengths of the composite films were increased proportionally via the addition of FA. The strength of the film was enhanced by 193% with 20% FA compared to the neat PVA control. Further addition of FA deviated from the linear trend. The moduli of the composites also increased proportionally with FA addition to 212% at 20 wt % FA addition compared to the control. The percentage strain at break exponentially decreased with the addition of FA. In the dynamic mechanical behavior, the storage and loss moduli both increased with FA content. The tan δ peaks corresponding to the glass-transition temperature shifted 5–10°C higher above the control sample (73°C). This shift was attributed to a reduction in the mobility of PVA segments because they were anchored by the FA surface. The reductions in mobility manifested in strong interfacial interactions were indicative of hydrogen bonding. Broadening and reduction in the intensities of the stretching and bending peaks of —OH, —CH and —C=O of PVA in the Fourier transform infrared spectra were observed. This suggested that hydrogen bonding was active between the functional groups in the FA and PVA chains. © 2010 Wiley Periodicals, Inc. J Appl Polym Sci 117: 114–121, 2010

Key words: biodegradable; composites; interfaces; strength

INTRODUCTION

Coal is burned in thermal power stations to generate electricity along with a vast amount of fine powder byproduct, known as *fly ash* (FA). The storage and handling of FA are ongoing challenges in the context of environmental impact. FA is commonly disposed as landfill in dams and lagoons. It typically consists of alkali and transition-metal oxides, mainly of silicon, aluminum, and iron, and a small percentage of calcium, magnesium, potassium, sodium, or titanium, depending on the processing conditions.[1,2]

Research on the recycling and reuse of FA as a filler in green and ecofriendly products and engineering composites has been considered for the past decade. The matrices that have been considered include metal[3] and polymers, such as polyester,[4] epoxy,[5] and polypropylene (PP).[6] Although petroleum-based PP makes a very popular thermoplastic with a moderately high strength, PP–FA composites properties are poor in tension. A dramatic loss in the tensile strength is observed with the addition of spherical particles of FA.[6]

In a recent study, higher mechanical strengths for FA-reinforced PP composites at elevated temperatures were observed;[7] however, the materials showed lower strengths with increasing FA addition at room temperature. This was suggested to be due to the absence of interfacial interaction between the PP and FA at room temperature. Estimations of the interfacial interactions derived from Punkanszky's equation gave depressed values. This indicated a likely weakening of the adhesion forces between nonfunctional PP and FA.[7] In studies of nonisothermal[8] and isothermal[9] crystallization kinetics, FA played role in the formation of new crystalline phases in PP chains. By forming stronger interfacial interactions, composite materials with improved rigidity and structural performance may be achieved. To this end, candidate base polymers and functional groups must be carefully selected to match FA addition.

A biodegradable and water-soluble biopolymer that has been regaining interest is poly(vinyl alcohol) (PVA). This polymer has been used in the formation of low-cost environmentally compatible composites

Correspondence to: S. Bandyopadhyay (s.bandyopadhayay@unsw.edu.au).

Contract grant sponsor: Australian Research Council (to D.C.D.N. through the Linkage program study); contract grant number: ARC LP0669837.

with sugar cane,[10] starch,[11] clay,[12] carbon nanotubes,[13] wood dust,[14] cement,[15] organoceramics,[16] and TiO_2.[17] PVA and its composites are used in a variety of forms and industrial applications, including in the fiber and textiles industries for sizing and finishing, coating, adhesives, emulsifiers, colloidal stabilizers, and film packaging in the food and optical holographic industries.[18]

PVA fibers reinforced with FA and FA–geopolymer board composites have recently been reported to achieve superior brittle-to-ductile transition performances and impact properties.[19,20] Considering the previous discussion, the objective of this study was to enhance the interfacial coupling between functional PVA and FA, which was strongly correlated to an enhancement in the mechanical strength of the composite films. Generally, the size and shape of the filler has a significant effect on the strength of the polymer composite. The nanosized clay particles dramatically increased all sorts of properties of the composite.[3]

EXPERIMENTAL

Materials

A sample of FA was obtained from Swanbank Coal Fire Plant (Cement Australia, Queensland, Australia). PVA (weight-average molecular weight = 125,000, degree of hydrolysis ≈89%) was purchased from Fine-Chemical, Ltd. (Chennai, India).

Preparation of the composite films

The composite films were fabricated by a casting method from an aqueous solution of PVA and FA. The neat PVA was dissolved in distilled water at 80°C to prepare a 1.2% solution. The FA particles with different concentration (5, 10, 15, 20, and 25%) were dispersed and sonicated for 5 min. The resulting mixtures were cast in glass Petri dishes, and bubbles were removed by shaking. The castings within the Petri dishes were kept at room temperature until they were completely dry. The films were peeled out and dried *in vacuo* in an oven at 60°C for 6 h. The thicknesses of the films were 0.05–0.07 mm. We controlled the thicknesses of the films by using the same amount of materials and glass Petri dishes. The total quantity of material for the uncrosslinked composite films was 400 mg of PVA and FA in 25 mL of distilled water.[11]

Testing and analytical instruments

A Coulter light-scattering particle size analyzer (USA) was used to determine the particle size and size distribution of FA, with water as a fluid and an experiment time of 60 s.

A Malvern light-scattering particle size analyzer (Worcestershire, UK) was also used to determine the particle size and distribution pattern of FA. The experiments were run for 60 s in water.

The chemical composition of FA was obtained with inductively coupled plasma/atomic emission spectroscopy (ICP–AES). A PANalytical PW 2400 sequential-wavelength, dispersive X-ray fluorescence (XRF) instrument (Almelo, The Netherlands) with an Rh end-window tube was used for XRF analysis. The samples were prepared as 40 mm glass beads with lithium metaborate as a fluxing agent. We calibrated the XRF for a wide range of elements with certified reference materials prepared as glass beads for major element oxides under ASTM D 6502-08 with optimum machine parameters and correcting for any spectral overlapping lines. We used Super Q software (Almelo, The Netherlands). All majors were expressed as oxides.

Wide-angle X-ray diffraction was carried out to investigate the crystal structure of FA. This was conducted in a multipurpose diffractometer (Almelo, The Netherlands) (Scherrer) with diffracted-beam graphite monochromators with Ni-filtered Cu Kα radiation. The diffractometer conditions for data collection were 40 kV and 20 mA, and a 2θ scanning range from 5 to 90° with a step size of 0.02 times per 0.5-s step. The qualitative phase analysis of FA was performed with a search/match tool in X'pert software program (Almelo, The Netherlands).

The mechanical properties, including tensile yield strength, strain at break, and modulus of elasticity, were determined from tensile tests with an Instron (Melbourne, Australia) 1185 instrument with a crosshead movement of 50 mm/min. The specimens were prepared as per ASTM D 882-95a (length = 22 mm, width = 5 mm) with samples cut by a sharp razor blade.[9,10] Four samples were tested in each category, and the results were averaged. The modulus values were calculated from the linear regions of the stress–strain curves without an extensometer.

Dynamic mechanical measurements were performed on 19 × 5 × 0.05-mm^3 film samples in tension–torsion mode between 25 and 150°C at a constant frequency of 1 Hz with a PerkinElmer (USA) dynamic mechanical analyzer. The heating rate was 2°C/min with a constant strain amplitude of 0.5%.

The composites were characterized by Fourier transform infrared spectroscopy (Nexus 870, Thermo Nicolet Corp., Berkeley, CA) run with Omnic software. The conditions for the measurement of Fourier transform infrared spectroscopy: MCT/A detector, KBr base splitter, diamond window, velocity = 0.6329, aperture = 100, resolution = 2 cm^{-1}, and 64 scans.

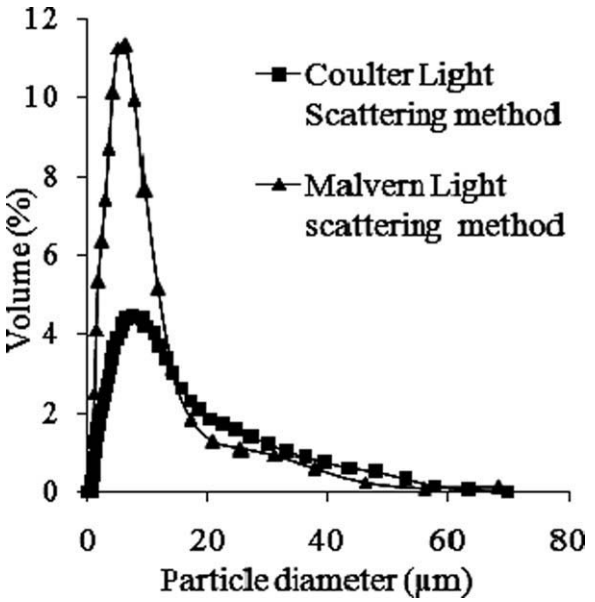

Figure 1 Particle size distribution of FA as determined with a light scattering size analyzer.

A Hitachi 4500-II scanning electron microscope (Blackwood, NJ) was used to examine the morphology of the FA and composites. The electrically nonconductive surfaces of the FA and composites (tensile-fractured films) were coated in a chromium sputter unit, with two coating cycles to improve the conductivity of the coating.

RESULTS AND DISCUSSION

Characterization of FA

The particle size distribution, determined separately by the Coulter and Malvern light-scattering methods, are displayed in Figure 1. Figure 1 shows a relatively narrow sharp peak between 0 and 20 μm. The scanning electron microscopy (SEM) image showed an irregular shape and craters on the surface of the FA particles, as shown in Figure 2.

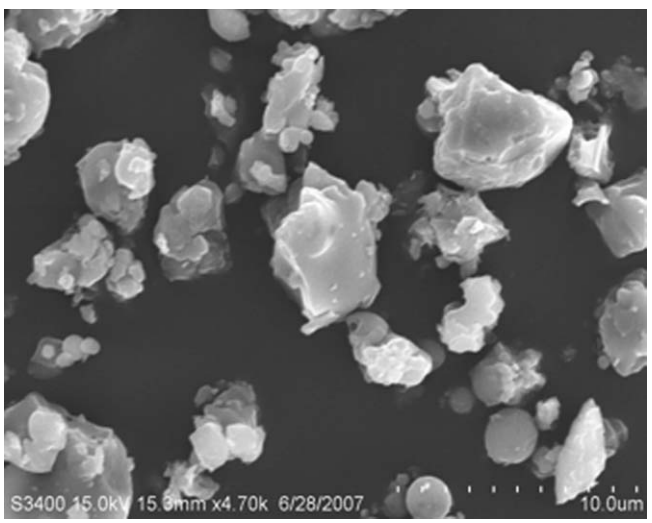

Figure 2 SEM image of the morphology of FA.

TABLE I
Chemical Composition of FA According to XRF and ICP–AES

Compound	XRF analysis	ICP–AES analysis
SiO_2	73.76	73.60
Al_2O_3	22.66	18.70
Fe_2O_3	0.91	1.90
CaO	0.43	1.02
MgO	0.54	0.46
TiO_2	1.54	1.36
BaO	—	0.06
Cr_2O_3	—	0.06
K_2O	0.32	0.27
MnO	0.54	0.01
Na_2O	0.64	1.00
P_2O_5	0.06	0.04
SrO	—	0.02
Loss on ignition	0.31	0.98
	100	100

The data from the chemical analysis of FA are listed in Table I. ICP–AES detected mainly Si_2O (73.60%), Al_2O_3 (18.70%), hematite (Fe_2O_3, 1.90%), and TiO_2 (1.36%), whereas XRF detected Si_2O (73.76%), Al_2O_3 (22.66%), Fe_2O_3 (0.91%), and TiO_2 (1.54%). Trace amounts of Cao, BaO, MgO, MnO, and P_2O_5 were common in both systems.

The mineralogical structure of FA was ascertained by wide-angle X-ray diffraction. The analysis of the spectra was accomplished by comparison to the standard authentic references downloaded in X-Pert Software and references. The spectra displayed in Figure 3 showed that the contents of FA were mainly hexagonal quartz [silicon dioxide (SiO_2)], orthorhombic mullite [aluminum silicate ($3Al_2O_3{\cdot}2SiO_2$)], Fe_2O_3, and magnetite (Fe_3O_4). These results agreed with a QEMSCAN analysis of FA, which showed predominantly about 70% aluminum silicate mullite and 10% silica phase (QEMSCAN is a computer software program used for the quantitative evaluation of mineral-phase analysis with automated SEM). Mullite was not an in ingredient of the sources of FA coal. The formation of mullet occurred in the process of the thermal decomposition of the mineral component kaolinite.[21]

Static mechanical properties of the neat PVA and composite films

The original stress–strain relationship diagrams of the neat PVA and composites with different concentrations of FA are presented in Figure 4, and the data are presented in Table II. The addition of FA to neat PVA enhanced the tensile strength proportionally, and a dramatic increase was observed at 15%

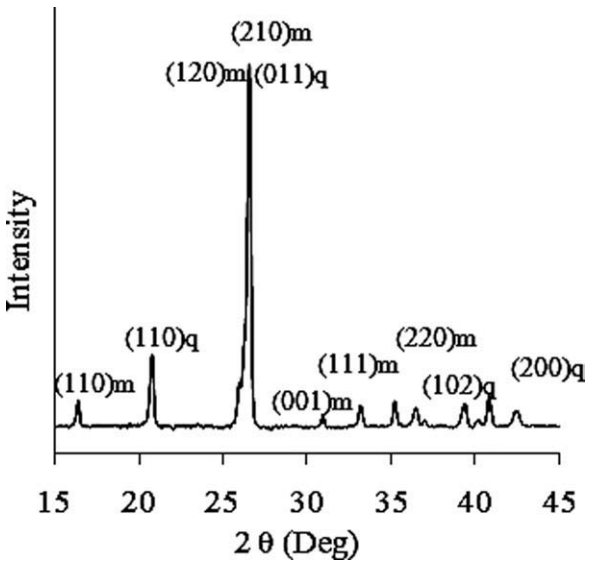

Figure 3 XRD of FA (m = mullite, q = quartz).

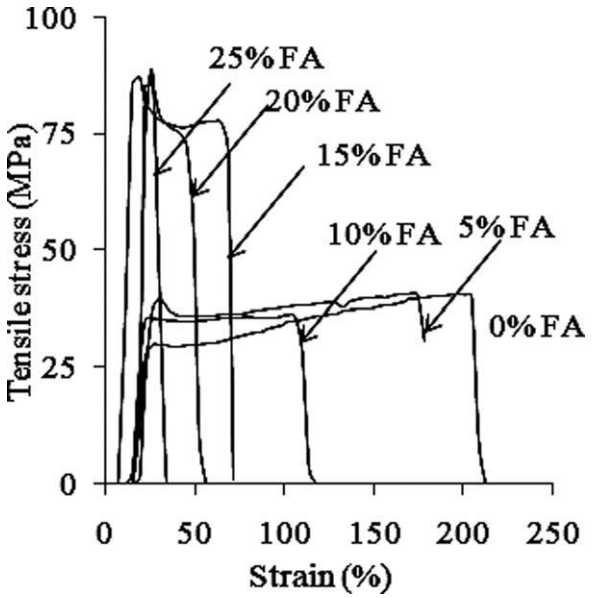

Figure 4 Stress–strain relationship of the neat PVA and composite films at 25°C.

FA, and further addition, such as 25%, gave a very slow subsequent increase.

Interestingly, when used as a composite with PP, FA decreased the tensile strength in the PP composite at room-temperature conditions.[6] The nonpolar PP was less likely to form an interfacial interaction zone to the FA surface physically and/or chemically. The formation of interfacial interactions between the two dissimilar low-molecular-weight molecules in the polymer composite played a key role in improving the mechanical strength compared to the neat polymer.[22]

PVA is a highly polar matrix containing —OH groups in addition to acetate groups. The molar quantities of functional groups in PVA chain depend on the degree of hydrolyzation during synthesis from polyvinyl acetate.[10] The 89% hydrolyzed PVA that was used in this study contained two major functional groups, —OH and —$COOCH_3$. Importantly, however, the functional —OH or ion generally covers the surfaces of metal and metalloid oxides. This plays a significant role in the formation of physical bonding between the surfaces of the substrates and —OH bonds present in fully hydroxylated silica powder as part of FA[23] because FA consists of about 74% silica. The existence of functional —OH groups on the surface of FA particles is expected to contribute to the composite's improved mechanical strength.[7] PVA is highly active in the formation of intramolecular and intermolecular hydrogen bonding between —OH groups.[24]

In the presence of FA, the existence of —OH groups on the particle surface may have taken part in the formation of hydrogen bonding between the PVA chain and FA. The degree of hydrogen bonding was correlated with the actual strength of the composites. At the 20% FA concentration, the maximum stoichiometric level of hydrogen bonding may have been attained between the FA surface and the PVA chains. The saturated level of interfacial interaction of the surfaces may have increased the tensile strength by transferring the load between PVA and FA and lessening the generation of local stress in the composite.[25] The strain may sequentially have decreased because of the fixing of the PVA chain to the solid support particles of FA, which rendered them less flexible under load.

The schematic diagram shown in Figure 5 was drawn to show the plausible features of hydrogen

TABLE II
Mechanical Properties of the Neat PVA and Composite Films

FA (%)	Tensile strength (MPa)	Strain (%)	Modulus (MPa)
0	28.2 ± 0.9	238 ± 10	120
5	35.7 ± 2	178 ± 5	140
10	37.4 ± 1	150 ± 7	156
15	79.8 ± 3	72 ± 2	256
20	85.8 ± 2	53 ± 3	374
25	88.4 ± 2	42 ± 2	334

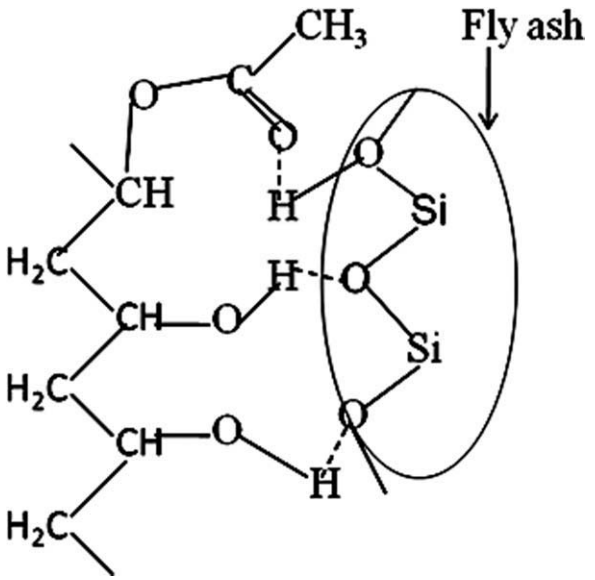

Figure 5 .Plausible diagram of hydrogen bonding between PVA and FA based on the tensile stress/strain profile and morphology of the composite films.

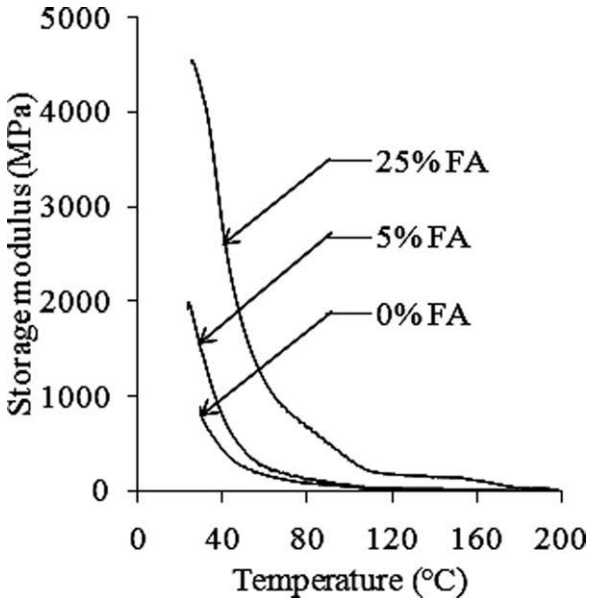

Figure 7 E' versus the temperature for the neat PVA and composite films with FA.

bonding. After exceeding the concentration, there may not have been additional sites to accommodate in the monolayer for the formation of bonding and to generate the particle–particle interaction. The particle–particle interaction failed to transfer the load and, hence, allowed the formation of local stress, which led to a crack initiation site that could result in catastrophic failure of the material.[22]

The relationship of the strain at break and modulus of the composite films with the FA content are plotted in Figure 6. The strains at break decreased and the modulus increased exponentially with the addition of FA; this illustrated the aforementioned explanations.

Dynamic mechanical properties of the neat PVA and composite films

The storage modulus (E'), loss modulus (E''), and tan δ of the neat PVA and composites are plotted against the test temperatures in Figures 7–9, respectively. The representative values of E' and E'' at different temperatures are shown in Tables III and IV, respectively. The magnitudes of the E' and E'' values

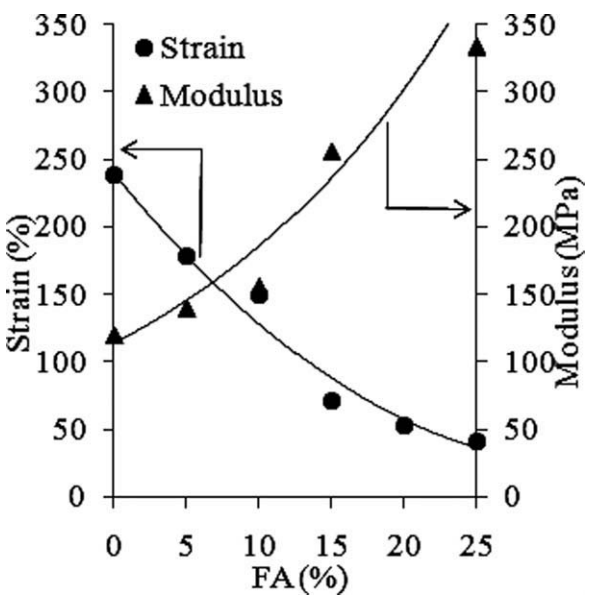

Figure 6 Relationship of the strain percentage and modulus of the neat PVA and composite films with the function of FA.

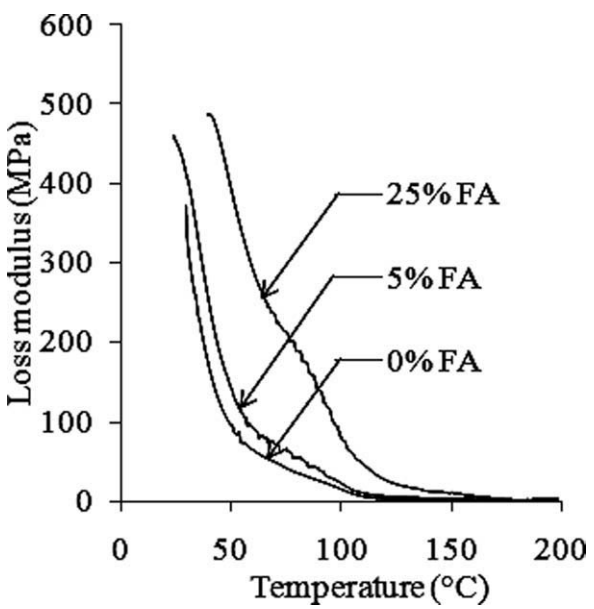

Figure 8 E'' versus the temperature for the neat PVA and composite films with FA.

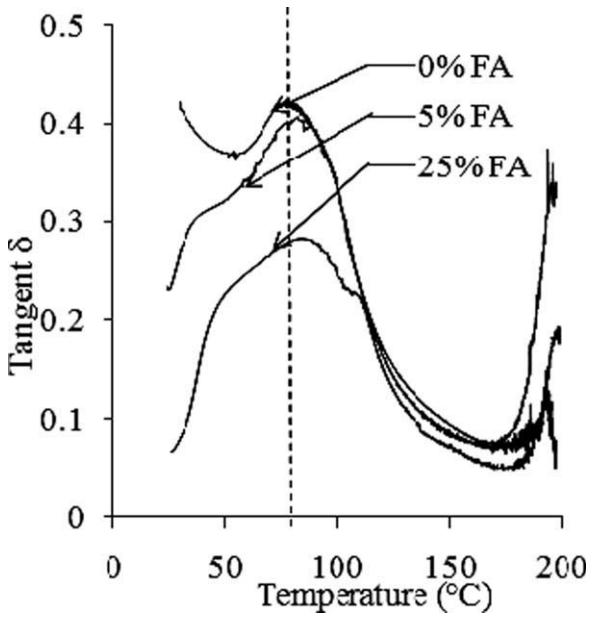

Figure 9 Tan δ versus the temperature for the neat PVA and composite films with FA.

of the composites in Figures 7 and 8 increased dramatically with the addition of 5–25% FA over the E' and E'' values of neat PVA at each temperature. Also, all curves displayed an exponential decrease with increasing test temperature associated with less constraint in the sliding of the polymer chains. The proportional increases in each curve with FA addition reflected the increasing degree of interfacial interaction between the surfaces of FA and PVA chains in the composite samples.

The E' and E'' values of all of the materials decreased slowly and formed a broadened inflection point, which reflected the glass-transition temperature of the amorphous domain in PVA.[26] In general, the sharpness and intensity of the loss peaks were greater in amorphous than in semicrystalline polymers. The uninhibited sliding of PVA segments were hypothesized to be interrupted by the FA addition and to fulfill two primary functions:

1. The generation of steric hindrance between the intersegments of PVA.
2. Linking of —OH groups to the PVA chains via hydrogen bonding.[24]

TABLE III
E' Values of the Neat PVA and PVA–FA Composites

	E' (MPa)				
FA (%)	40°C	60°C	80°C	100°C	120°C
0	448.0	174.6	87.2	45.5	22.0
5	818.2	267.8	133.5	66.7	31.7
25	2808.1	1163.9	676.8	328.3	177.6

TABLE IV
E'' Values of the Neat PVA and PVA–FA Composites

	E'' (MPa)				
FA (%)	40°C	60°C	80°C	100°C	120°C
0	172.3	65.5	36.3	16.1	3.6
5	251.9	92.1	53.9	22.2	5.5
25	486.4	290.3	189.8	80.4	26.9

As a result, the magnitudes of E' and E'' increased in films with FA addition. The tan δ values of the neat PVA and composites increased as a function of temperature and reached a maximum level, which was by definition the glass-transition temperature of the amorphous phase in the polymer.[26] For neat PVA, as shown in Figure 9, this temperature was approximately 73°C, and for the composites, the value increased between 5 and 10°C. This indicated that the restriction of the segmental motion of PVA necessitated additional energy to shift the amorphous domains within the PVA matrix because of the formation of interfacial interactions between PVA and FA.[27]

Characterization of the composite films

The structural features of the neat PVA and the composites were investigated by infrared spectroscopy, and the spectra are displayed in Figure 10. The selected peaks were assigned with the help of refs. 11, 17, 24, 28, and 29 and are displayed in Table V. A broad absorption band was centered at 3298 cm^{-1}, which reflected the combination of —OH groups in

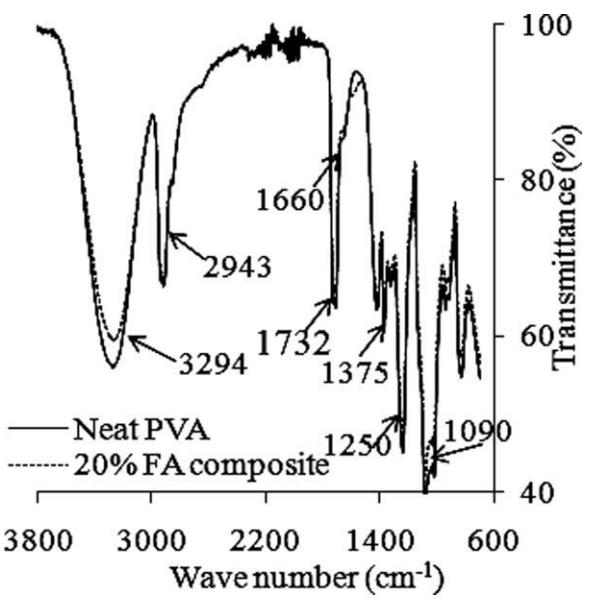

Figure 10 Infrared spectra of the neat PVA and composite films showing the shifting of the absorption band of chemical bonds with decreasing intensity.

TABLE V
Selected Fourier Transform Infrared Absorptions of the Neat PVA and Composite Films

Sample	Peak positions of the structural groups (cm^{-1})						
	OH stretching	C—H stretching/bending	C=O stretching	O—H bending	C—H bending	C—O—C stretching	C—OH stretching
PVA	3298	2924/2875	1732	1419	1375	1250	1090
PVA + 20% FA	3263	2902/2873	1718	1412	1377	1248	1082

the PVA and adsorbed water.[28] The well-known set of absorption bands at 3298 cm^{-1} of —OH stretching, 2924 and 2875 cm^{-1} of C—H stretching, 1732 cm^{-1} of C=O stretching, 1419 and 1375 cm^{-1} of —O—H/C—H bending, and 1080 cm^{-1} of C—O—H stretching appeared in neat PVA.[29] All of the peaks of the PVA molecules in the composite with FA were significantly shifted to lower wave numbers along with slightly lower intensities; this indicated the existence of possible intermolecular and/or intramolecular hydrogen bonding between FA and PVA,[24] which was related to the plausible hydrogen bonding of PVA and FA shown in Figure 5:

1. Between C=O groups in PVA and —OH groups on the surface of the FA particles.[15]
2. Between —OH groups in PVA and Si—O groups on the FA surface.[29]

The hydrogen bonding partially anchored the high-modulus FA particles to the segments of PVA. This, thereby, restricted the mobility of PVA and

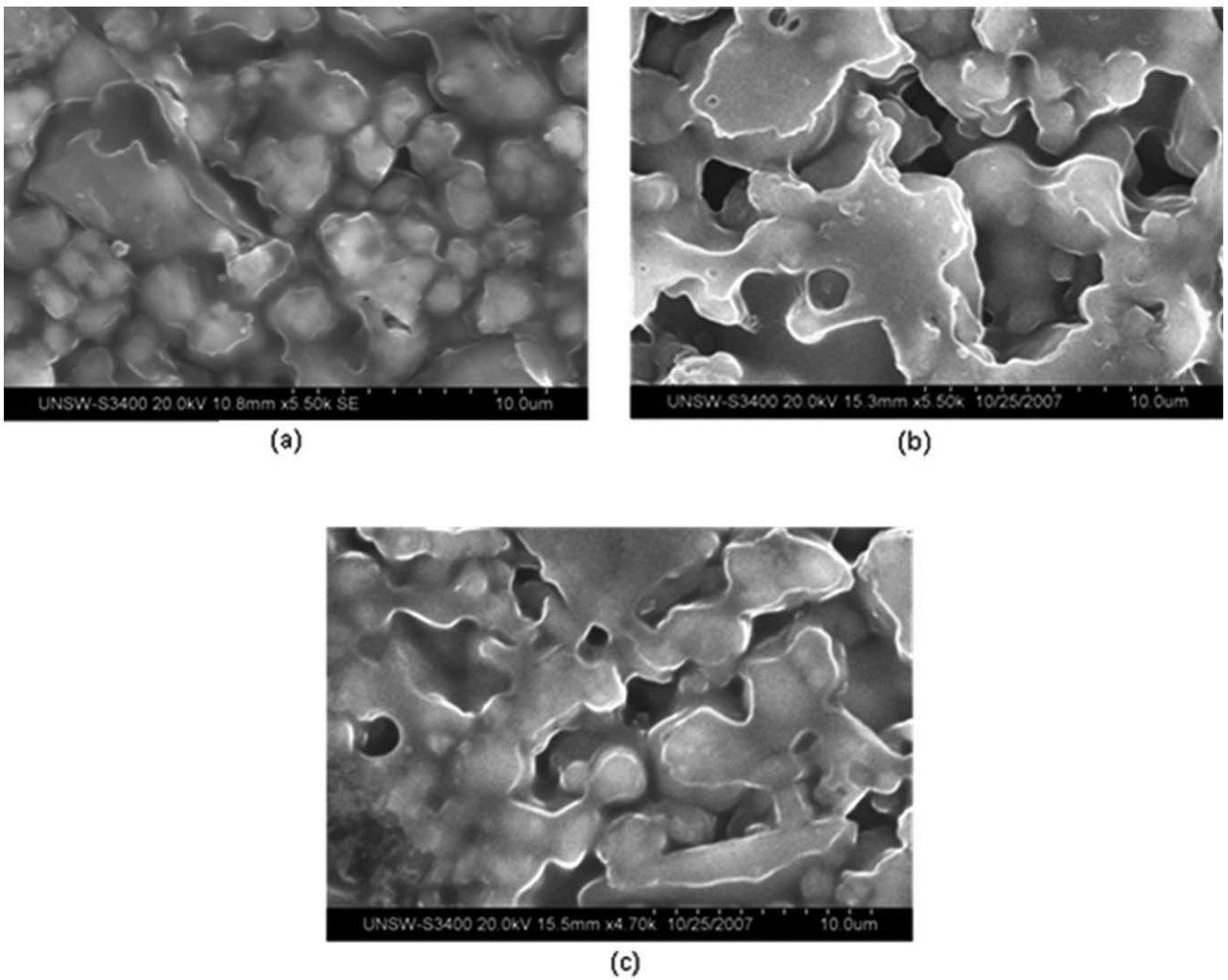

Figure 11 SEM images of the morphology of the composite films showing a connection: (a) 10, (b) 20, and (c) 25% FA.

resulted in the reduction of ductility under load and negotiated efficient load transfer between the FA and PVA. The FA surface reactions produced strong covalent Si—O—C bridges with the PVA of the matrices. The initial mobility of the PVA chains was thus constrained when they were subjected to a mechanical load.

Morphology of the composite films

The representative SEM images of the 10, 20, and 25% FA composite films are displayed in Figure 11. The finely dispersed FA particles were thoroughly wetted and encompassed by the PVA chains; this facilitated intimate contact. The entire micrograph showed the efficient packing of FA in the composites with only a few interstitial voids.[16] The connections allowed stress transfer between the FA and PVA chains under tensile stress. In the absence of interstitial voids, the composites had less possibility of local stress concentrations, which thus reduced the onset of crack extension. In terms of elongation behavior, the interconnectivity of the composite strongly inhibited the mobility of the segmental polymer chains and resulted in a reduction in the elongation when compared to the neat matrix.[30] It was by these mechanisms that the PVA–FA composite materials were able to exhibit higher tensile strengths and reduced elongations. Thus, by the addition of FA waste product, a low-cost biodegradable polymer was modulated into an engineering composite candidate.

CONCLUSIONS

There is a growing trend toward the development of competent biodegradable composites with low environmental impact and good commercial viability. This study outlined the preparation and characterization of FA-filled PVA composite films. The key points from this study are as follows:

1. The spherical FA particles were finely dispersed in the PVA matrix; this resulted in a proportional increase in the tensile strength. The maximum strength was attained with the addition of 20 wt % FA. Further FA addition led to a reduction in intimate contact between the surfaces of FA and PVA.
2. A physical bond was achieved at the PVA–FA interface; this led to efficient load transfer and the preclusion of stress localizations. The interfacial bonding was proposed to predominantly consist of hydrogen bonding.
3. E' and E'' of the composite materials displayed similar increasing trends with the addition of FA as a function of temperature. The tan δ curves of the composite films shifted by 10°C compared to neat PVA; this indicated a higher glass-transition temperature and strong interfacial interactions between the FA and PVA chains.
4. The morphology and topography of the biodegradable composites were assessed by SEM. The SEM micrographs clearly indicated wetting, intimate bonding, and the connection of FA particles with the PVA matrix.

References

1. Ward, C. R.; French, D. Fuel 2006, 85, 2268.
2. Alkan, C.; Arslan, M.; Cici, M.; Kaya, M.; Aksoy, M. Resour Conserv Recycl 1995, 13, 147.
3. Kojima, Y.; Usuki, A.; Kawasumi, M.; Fukushima, Y.; Okada, A.; Kurauchi, T.; Kamigaito, O. J Mater Res 1993, 8, 1179.
4. Guhanathan, S.; Sarojadevi, M. Compos Interface 2004, 11, 43.
5. Gupta, N.; Brar, B. S.; Woldesenbet, E. Bull Mater Sci 2001, 24, 219.
6. Wong, K. W. Y.; Truss, R. W. Compos Sci Technol 1994, 52, 361.
7. Nath, D. C. D.; Bandyopadhyay, S.; Yu, A.; Zeng, Q.; Das, T.; Blackburn, D.; White, C. J Mater Sci 2009, 44, 6078.
8. Nath, D. C. D.; Bandyopadhyay, S.; Yu, A.; Blackburn, D.; White, C. J Appl Polym Sci 2010, 115, 1510.
9. Nath, D. C. D.; Bandyopadhyay, S.; Yu, A.; Blackburn, D.; White, C.; Varughese, S. J Therm Anal Calorim, to appear.
10. Chiellini, E.; Cinelli, P.; Imam, S. H.; Mao, I. Biomacromolecules 2001, 2, 1029.
11. Ramaraj, B. J Appl Polym Sci 2007, 103, 909.
12. Strawhecker, K. E.; Manias, E. Chem Mater 2000, 12, 2943.
13. Zhang, X.; Liu, T.; Sreekumar, T. V.; Kumar, S.; Moore, V. C.; Hauge, R. H.; Smalley, R. Nano Lett 2003, 3, 1285.
14. Bana, R.; Banthia, A. K. Polym Plast Technol Eng 2007, 46, 821.
15. Weichold, O.; Moller, M. Adv Eng Mater 2007, 9, 712.
16. Tan, L. S.; McHugh, A. J. J Mater Sci 1996, 31, 3701.
17. Chen, X. J Mater Sci Lett 2002, 21, 1637.
18. Huang, H.; Gu, L.; Ozaki, Y. Polymer 2006, 47, 3935.
19. Sun, P.; Wu, C. H. Cem Concr Compos 2008, 30, 29.
20. Yunseng, Z.; Wei, S.; Zongjin, L. J Mater Sci 2006, 41, 2787.
21. Gorninski, J. P.; Molin, D. C. D.; Kazmierczak, C. S. Cem Concr Res 2004, 34, 2091.
22. Tjong, S. C.; Li, R. K. Y.; Cheung, T. Polym Eng Sci 1997, 37, 166.
23. Mueller, R.; Kammler, H. K.; Wegner, K.; Pratsinis, S. E. Langmuir 2003, 19, 160.
24. Huang, H.; Gu, L.; Ozaki, Y. Polymer 2006, 47, 3935.
25. Bigg, D. M. Polym Compos 1987, 8, 115.
26. Doan, T. T. L.; Brodowsky, H.; Mader, E. Compos Sci Technol 2007, 67: 2707.
27. Bandi, S.; Schiraldi, D. A. Macromolecules 2006, 39, 6537.
28. Yurudu, C.; Isci, S.; Unlu, C.; Atici, O.; Ece, I.; Gungor, N. J Appl Polym Sci 2006, 102, 2315.
29. Kaczmarek, H.; Podgorski, A. J Photochem Photobiol A 2007, 191, 209.
30. Leong, Y. W.; Bakar, M. B. A.; Ishak, Z. A. M.; Ariffin, A.; Pukanszky, B. J Appl Polym Sci 2004, 91, 3315.